[12] J. Hofkens, M. Maus, T. Gensch, T. Vosch, M. Cotlet, F. Köhn, A. Herrmann, K. Müllen, F. C. De Schryver, *J. Am. Chem. Soc.* **2000**, *122*, 9278.

[13] J. Hofkens, L. Latterini, G. De Belder, T. Gensch, M. Maus, T. Vosch, Y. Karni, G. Schweitzer, F. C. De Schryver, A. Herrmann, K. Mullen, *Chem. Phys. Lett.* **1999**, *304*, 1.

[14] Y. Karni, S. Jordens, G. De Belder, G. Schweitzer, J. Hofkens, T. Gensch, M. Maus, F. C. De Schryver, A. Herrmann, K. Mullen, *Chem. Phys. Lett.* **1999**, *310*, 73.

[15] Y. Karni, S. Jordens, G. De Belder, J. Hofkens, G. Schweitzer, F. C. De Schryver, *J. Phys. Chem. B* **1999**, *103*, 9378.

[16] T. Weil, U. M. Wiesler, A. Herrmann, K. Mullen, *J. Am. Chem. Soc.* **2000**, submitted.

[17] F. Morgenroth, E. Reuther, K. Mullen, *Angew. Chem.* **1997**, *109*, 647; *Angew. Chem. Int. Ed. Engl.* **1997**, *36*, 631.

[18] F. Morgenroth, K. Mullen, *Tetrahedron* **1997**, *53*, 15349.

[19] F. Morgenroth, C. Kubel, M. Muller, U. M. Wiesler, A. J. Berresheim, M. Wagner, K. Mullen, *Carbon* **1998**, *36*, 833.

[20] V. Gulbinas, L. Valkunas, D. Kuciauskas, E. Katilius, V. Liuolia, W. L. Zhou, R. E. Blankenship, *J. Phys. Chem.* **1996**, *100*, 17950.

[21] L. Valkunas, V. Gulbinas, *Photochem. Photobiol.* **1997**, *66*, 628.

[22] V. Barzda, G. Garab, V. Gulbinas, L. Valkunas, *Biochim. Biophys. Acta Bioenerg.* **1996**, *1273*, 231.

[23] W. H. J. Westerhuis, M. Vos, R. van Grondelle, J. Amesz, R. A. Niederman, *Biochim. Biophys. Acta Bioenerg.* **1998**, *1366*, 317.

[24] A. Ruseckas, M. Theander, L. Valkunas, M. R. Andersson, O. Inganas, V. Sundstrom, *J. Lumin.* **1998**, *76 – 77*, 474.

[25] V. Sundstrom, T. Gillbro, R. A. Gadonas, A. Piskarskas, *J. Phys. Chem.* **1988**, *89*, 2754.

[26] I. G. Scheblykin, O. P. Varnavsky, M. M. Bataiev, O. Sliusarenko, M. Van der Auweraer, A. G. Vitukhnovsky, *Chem. Phys. Lett.* **1998**, *298*, 341.

[27] M. Maus, S. Mitra, M. Lor, T. Weil, J. Hofkens, K. Mullen, F. C. De Schryver, submitted.

[28] D. J. Nesbitt, R. W. Field, *J. Phys. Chem.* **1996**, *100*, 12735.

[29] J. S. Baskin, L. Banares, S. Pedersen, A. H. Zewail, *J. Phys. Chem.* **1996**, *100*, 11920.

[30] T. Nakabayashi, H. Okamoto, M. Tasumi, *J. Phys. Chem. A* **1997**, *101*, 3494.

[31] I. V. Rubtsov, K. Yoshihara, *J. Phys. Chem. A* **1999**, *103*, 10202.

[32] H. Zhang, A. M. Jonkman, P. van der Meulen, M. Glasbeek, *Chem. Phys. Lett.* **2000**, *224*, 551.

[33] M. L. Horng, J. A. Gardecki, A. Papazyan, M. Maroncelli, *J. Phys. Chem.* **1995**, *99*, 17311.

[34] G. Schweitzer, G. De Belder, S. Jordens, Y. Karni, F. C. De Schryver, unpublished results.

[35] R. M. Stratt, M. Maroncelli, *J. Phys. Chem.* **1996**, *100*, 12981.

[36] P. K. McCarthy, G. J. Blanchard, *J. Phys. Chem.* **1996**, *100*, 14592.

[37] T. Gustavsson, G. Baldacchino, J. C. Mialocq, S. Reekmans, *Chem. Phys. Lett.* **1995**, *236*, 587.

[38] W. Jarzeba, G. C. Walker, A. E. Johnson, M. A. Kahlow, P. F. Barbara, *J. Phys. Chem.* **1998**, *92*, 7039.

[39] Y. Kimura, J. C. Alfano, P. K. Walhout, P. F. Barbara, *J. Phys. Chem.* **1994**, *98*, 3450.

[40] L. Reynolds, J. A. Gardecki, S. J. V. Frankland, M. L. Horng, M. Maroncelli, *J. Phys. Chem.* **1996**, *100*, 10337.

[41] P. Changenet, P. Plaza, M. M. Martin, Y. H. Meyer, *J. Phys. Chem. A* **1997**, *101*, 8186.

[42] P. Changenet, H. Zhang, M. J. van der Meer, K. J. Hellingwerf, M. Glasbeek, *Chem. Phys. Lett.* **1998**, *282*, 276.

[43] R. D. Harcourt, K. P. Ghiggino, G. D. Scholes, R. P. Steer, *J. Chem. Phys.* **1998**, *109*, 1310.

[44] G. Paillotin, C. E. Swenberg, J. Breton, N. E. Geacintov, *Biophys. J.* **1979**, *25*, 513.

[45] G. Schweitzer, L. Xu, B. Craig, F. C. De Schryver, *Opt. Commun.* **1997**, *142*, 283.

Effects of Oxidation on the Nanoscale Mechanisms of Crack Formation in Aluminum**

Emily A. A. Jarvis,[a] Robin L. Hayes,[a] and Emily A. Carter*[a]

Materials failure, in the form of cracking, is a phenomenon of fundamental scientific interest and one that impacts a variety of applications spanning a wide range of fields, particularly those of materials science and engineering. Experiments have investigated extensively the macroscopic properties associated with cracking within homogeneous materials as well as at interfaces between dissimilar materials. Likewise, theoretical modeling via engineering finite-element approaches[1] and molecular dynamics simulations with empirical embedded-atom potentials[2, 3] have provided some insight into cracking mechanisms. Nevertheless, these models rely on inherent assumptions concerning interatomic and/or bulk behavior, a drawback in instances where fundamental atomic interactions are poorly understood or improperly characterized by overly simplified model potentials. A comprehensive study incorporating a first principles approach at the atomic scale and effectively linking this information to the macroscopic scale poses an array of challenges, implementational and otherwise. To date, these difficulties and the computational expense associated with first principles calculations have generally motivated employing empirical assumptions to treat mechanics of the smallest length-scale regime. Resorting to empirical models limits the chemistry that may be accounted for. Accordingly, despite widespread scientific interest in the cracking phenomenon, aspects of the microscopic failure mechanisms remain largely a mystery. Herein, we investigate some aspects of the atomic-level properties which lead to chemically induced crack formation within a simple model. Finding methods to smoothly and effectively couple microscopic to macroscopic modeling is an active area of research[4, 5] and will provide much-needed insight into a complete mechanism for chemically induced cracking.

Aluminum is an important engineering material used in a variety of applications; to understand its behavior under stress is essential. Under ambient conditions, a self-limiting oxide layer forms on the aluminum surface and protects the underlying metal from further oxidation. This, in addition to their light

[a] *Prof. E. A. Carter, E. A. A. Jarvis, R. L. Hayes*
Department of Chemistry and Biochemistry
University of California, Los Angeles
Los Angeles, CA 90095-1569 (USA)
Fax: (+ 1)310-267-0319
E-mail: eac@chem.ucla.edu

weight and strength, makes aluminum alloys popular materials from which to fabricate, for example, airplane components.[6] Since the oxidation of aluminum affects its mechanical strength, it may prove critical to account for such effects in a simulation of crack growth. Accordingly, we consider a simple model of the effect of oxidation on crack formation by examining, at the atomic level, how cracks form in aluminum and its fully oxidized, stable partner α-Al$_2$O$_3$. More specifically, we calculate the dependence of the crystal energies upon tensile stress applied perpendicular to the face-centered cubic (fcc) Al (111) planes and hexagonal α-Al$_2$O$_3$ (0001) planes, also known as the basal plane of alumina. These planes were chosen since the most energetically favorable, low-index surfaces of aluminum are those parallel to the (111) planes[7] and Al$_2$O$_3$ formed from the oxidized metal has been shown to grow with surfaces parallel to the (0001) planes.[8]

Using periodic slab density functional theory (DFT)[9, 10] within the generalized gradient approximation (GGA),[11, 12] we investigate crack formation in α-Al$_2$O$_3$ and aluminum.[13] To simulate crack formation, we introduce a region of vacuum parallel to the bulk (0001) planes for α-Al$_2$O$_3$ and the bulk (111) planes for Al and allow the atomic coordinates of the system to relax from that starting point. We perform a series of such calculations, introducing successively wider regions of vacuum until the relaxed system energetics are equivalent to those of isolated surfaces.

[*] Members of the Editorial Advisory Board will be introduced to the readers with their first manuscript.

Figure 1 a shows the area-normalized energy increase relative to the bulk crystal with respect to width of vacuum introduced, namely, the initial crack separation. The initial steep slope represents a region where relaxed atoms of the material uniformly expand to heal the crack. Conversely, the region with small slope corresponds to the situation where the vacuum is
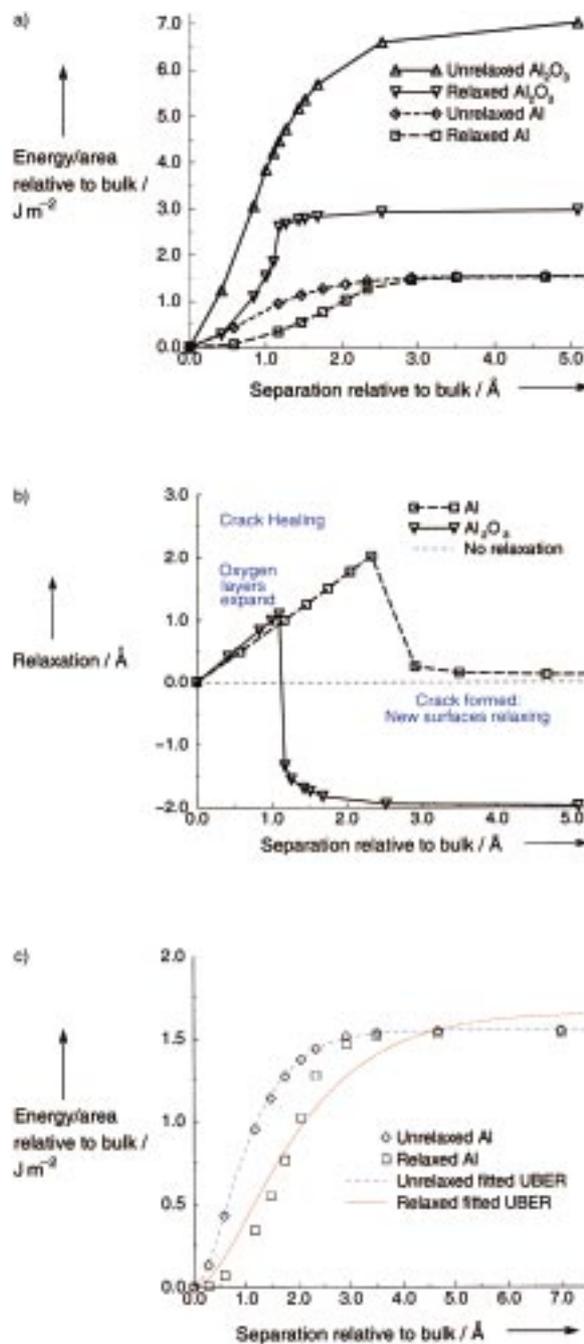
Figure 1. *a) Energy versus separation relative to the bulk for α-Al$_2$O$_3$ and Al with values for both initial (unrelaxed) atomic coordinates and final (relaxed) atomic coordinates. Separation refers to the width of crack introduced (zero separation represents the bulk equilibrium structure). b) Relaxation versus initial separation relative to the bulk for α-Al$_2$O$_3$ and Al. Zero relaxation represents the bulk equilibrium interlayer spacing. c) Comparison of UBER curves and our values (the same as (a)) obtained for Al crack formation. The fits from UBER for both the relaxed and unrelaxed structures involved separate optimization of the UBER parameters.*

too large for crack healing to occur upon relaxation; instead, the system is forced to form a surface on either side of the crack. The calculated surface energy of α-Al_2O_3 is much higher than that of aluminum; it is greatly affected by relaxation of atomic coordinates due to unfavorable "bare" $Al^{\sim 3+}$ on the initially cleaved surface. Upon relaxation, the Al cations relax toward the plane of oxygen atoms, as has been noted previously.[14–18] From this plot, we can estimate the cleavage energy, which is the energy required to form a crack in each material, from the energy increase, relative to bulk, of the relaxed structure immediately after a nonhealing crack is formed. For Al_2O_3, this occurs at a separation of 1.2 Å with a cleavage energy of 2.6 J m^{-2} relative to the bulk, while the cleavage energy of aluminum is much lower, 1.5 J m^{-2} at a separation of 2.9 Å. Although the significantly higher value of α-Al_2O_3 compared to Al may seem counterintuitive, recall the present discussion is limited to *ideal cleavage energetics* that do not account for effects such as dislocation nucleation, inherent to ductile cracking. Creating such transient defects permits macroscopic aluminum to appear much "stronger" due to its more efficient dissipation of crack-tip energy via such mechanisms; the inclusion of macroscopic energy dissipation is essential for a macroscopic strength estimate. On the other hand, dislocations are less likely to form in Al_2O_3, due to the rigidity of ceramic materials, and hence the cleavage energy calculated here for Al_2O_3 may be realistic. While Al_2O_3 appears "stronger" than Al when no dissipative mechanisms are allowed, its brittleness results in crack formation on a much shorter separation length scale, as we now describe.

In Figure 1b, we plot the relaxation of surface atomic coordinates from their bulk value with respect to the width of the vacuum region introduced. This figure dramatically displays the greater extent of the separation region over which Al, relative to Al_2O_3, is able to heal the introduced crack. Such behavior is indicative of ductile versus brittle materials failure. The α-Al_2O_3 forms cracks when only 1.2 Å of vacuum is introduced, whereas Al is able to heal cracks over 2.3 Å wide! The interlayer spacing in bulk aluminum is also 2.3 Å, so this introduced vacuum results in an interlayer separation of 4.6 Å over which the Al crystal can heal. The interlayer spacing between the Al in α-Al_2O_3 is 0.5 Å, hence the crystal is only able to heal over an interlayer separation of ~ 1.6 Å. The Al(111) surface expands slightly (1.5 %) upon relaxation for large separations, consistent with experimental observations.[19, 20] As explained for Figure 1a, the Al_2O_3(0001) surface experiences dramatic inward relaxation. A surface is created on both sides of the crack; accordingly, this plot indicates twice the surface relaxation.

While the aluminum crack can heal even with introduction of a void larger than 2.3 Å, the Al_2O_3 can only heal across crack widths of ≤ 1.1 Å. Figure 2 provides an explanation for this observation with plots of valence electron density. The highly localized electron density of the ionic crystal α-Al_2O_3 appears in sharp contrast to the delocalized (metallic) electron density of aluminum.[*] The electron density extending across the vacuum
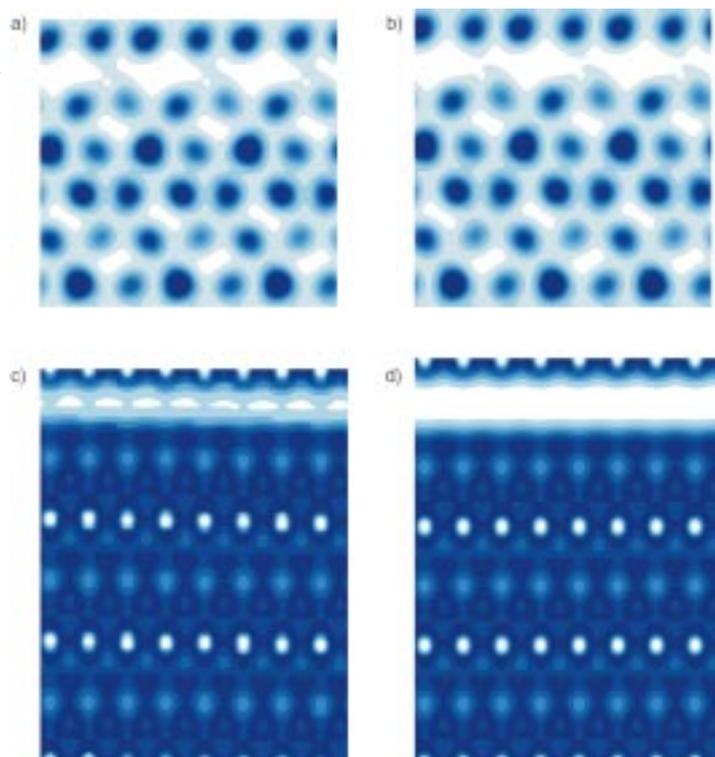
Figure 2. *Valence electron-density plots for α-Al_2O_3 and aluminum. Dark values indicate regions of highest density. (To facilitate ease of visualization, due to the high values of the localized electron density on oxygen, the α-Al_2O_3 plots show ten equivalent contours whereas the corresponding aluminum plots only have six contours.) a) Al_2O_3 unrelaxed structure with 1.0 Å vacuum introduced. Note the continuity of electron density across the crack. This crack heals upon relaxation. b) Al_2O_3 unrelaxed structure with 1.2 Å vacuum introduced. Note the lack of electron density bridging the crack. This crack further separates (does not heal) upon relaxation. c) Aluminum unrelaxed structure with 2.1 Å vacuum introduced. Note the continuous shaded area of low electron density bridging the crack. This crack heals upon relaxation. d) Aluminum unrelaxed structure with 2.9 Å vacuum introduced. Note the lack of electron density connecting the two surfaces. This crack does not heal upon relaxation.*

region in Al_2O_3 shows a dramatic decline going from 1.0 Å to 1.2 Å of introduced vacuum (Figures 2 a and b). By contrast, such a decline is observed for Al only beyond 2.0 Å vacuum. The behavior associated with relaxing metal surfaces in close proximity, namely the "avalanche" effect or "jump to contact",[21–24] is related to the extent of the electron density into the vacuum. The contrast in decay rate of the electron density between insulators and metals is central to the atomic-level reasons for brittle versus ductile behavior. The long range of the density falloff in the metal allows atomic-scale preference for alternate modes of energy dissipation, namely, atomic "stretching" to bridge the void. Naturally, at the macroscopic level, further evidence for ductile behavior is shown by the preference for forming dislocation planes over crack-tip propagation.

Although such behavior of the electron density has not been previously compared for the specific systems of Al_2O_3 and Al, it is a result anticipated from understanding electron-density decay as a function of the relative band gap in the crystal.[25–27] A previous study designed to model the (111) surfaces of the semiconductor Si showed a decline of electron density roughly

intermediate to the void widths required for "cracking" of our insulating and metallic systems.[28] A much earlier series of studies on metal adhesion, including that of aluminum, displayed a "strong bonding" range of roughly 2 Å.[29] Recently, Ismail-Beigi et al. derived a simple empirical approximation to the electron-density decay for metals and crystals with relatively small bandgaps. However, this same study concluded that for tightly bound insulators,[**] a simple analytical form to describe the spatial decay of the electron density is not readily obtainable; rather, it strongly depends on specifics of the atomic potentials in the crystal.[30] This highlights the importance of a high quality materials description at the atomic scale, even when one is interested in macroscopic phenomena.

The so-called universal binding energy–distance relationship (UBER) is a popular empirical relation, purported to describe cohesion and adhesion of metals, that has been shown to capture the essential features of the energy versus separation curve for a variety of covalent diatomic species and unrelaxed metal surfaces.[31] An attempt to describe ionic crystals, related in spirit to the UBER, has been proposed but has been limited to very simple crystals in application.[32] Just as generic analytical forms for the decay of the electron density are inadequate for tightly bound insulators, so too the UBER is unable to capture the features of relaxed energy versus separation curves. Although the UBER works fairly well for rigidly separated cracks in metals, obtaining a good UBER fit is not possible when surface relaxation is allowed. For example, Figure 1 c displays our UBER fits for both the unrelaxed and relaxed aluminum data sets. The two parameters in the UBER were varied to obtain optimal fits. Given the small surface relaxation in aluminum compared to Al_2O_3 and that the UBER was only claimed to be applicable to metals and covalently bonded diatomic species,[31] this should have been the optimal case for the UBER to be successful. The large relaxation of the Al_2O_3 surface and the ionicity of the crystal make it a very poor candidate for the UBER approximation. Nevertheless, despite the relatively "ideal" properties of aluminum for application of the UBER, the approximation breaks down with inclusion of surface relaxation. Similar limitations in the UBER approximation apply to previous theoretical studies of the adhesive "avalanche"[21–24, 28] and in attempts to model experimentally observed behavior between an STM tip and an Al surface.[33, 34] This provides further incentive for use of ab initio data as input to continuum models, since surface relaxation will occur on the time scales for most mechanisms of crack propagation.[35]

In sum, we find that the sharp falloff in electron density at Al_2O_3 surfaces provides a nanoscale explanation for the brittleness of alumina, since cracks form after the lattice experiences small expansions that correspond to loss of "bridging" electron density across the crack. Moreover, the large structural relaxation of Al_2O_3 surfaces inhibits healing of small cracks, once they are formed. This structural relaxation diminishes the acceptability of simple interaction models in macroscale simulations and suggests such relaxation should be accounted for in the future.

[**] *"Tightly bound insulator" refers to a crystal with a band gap greater than or equal to the valence bandwidth.*

Finally, this work implies that the oxidation of aluminum enhances both crack initiation at Al surfaces—due to the brittle behavior of Al_2O_3—and perhaps crack propagation, since ambient air will oxidize both the crack tip leading edge and its surfaces, to render cracking into the bulk more facile.

[1] J. R. Rice, D. E. Hawk, R. J. Asaro, *Int. J. Fract.* **1990**, *42*, 301–321.

[2] Y. Sun, J. R. Rice, L. Truskinovsky in *High Temperature Intermetallic Alloys*, Vol. 213 (Eds.: L. A. Johnson, D. T. Pope, J. O. Stiegler), MRS, Pittsburgh, **1991**, pp. 243–248.

[3] Y. Sun, G. E. Beltz, J. R. Rice, *Mater. Sci. Eng. A* **1993**, *170*, 67–85.

[4] F. F. Abraham, J. Q. Broughton, N. Bernstein, E. Kaxiras, *Europhys. Lett.* **1998**, *44*, 783–787.

[5] A. G. Evans, J. W. Hutchinson, Y. Wei, *Acta Mater.* **1999**, *47*, 4093–4113.

[6] M. L. Du, F. P. Chiang, S. V. Kagwade, C. R. Clayton, *Int. J. Fatigue* **1998**, *20*, 743–748.

[7] J. T. Klomp, *Mater. Res. Soc. Symp. Proc.* **1985**, *40*, 381–391.

[8] E. M. Clausen, Jr., J. J. Hren, *Mater. Res. Soc. Symp. Proc.* **1985**, *41*, 381–386.

[9] P. Hohenberg, W. Kohn, *Phys. Rev. B* **1964**, *136*, 864–871.

[10] W. Kohn, L. J. Sham, *Phys. Rev. A* **1965**, *140*, 1133–1138.

[11] J. P. Perdew in *Electronic Structure of Solids* (Eds.: P. Ziesche, H. Eschrig), Akademie Verlag, Berlin, **1991**, p. 11.

[12] J. P. Perdew, J. A. Chevary, S. H. Vosko, K. A. Jackson, M. R. Pederson, D. J. Singh, C. Fiolhais, *Phys. Rev. B* **1992**, *46*, 6671–6687.

[13] We performed DFT calculations within the generalized gradient approximation (PW91) to the exchange–correlation potential using the Vienna Ab Initio Simulation Package [G. Kresse, J. Hafner, *Phys. Rev. B* **1993**, *47*, 558–561; G. Kresse, J. Furthmüller, *Comput. Mater. Sci.* **1996**, *6*, 15–50]. Our calculations employed ultrasoft pseudopotentials to replace the core electrons; nonlinear core corrections to exchange and correlation were included for Al. We tested for convergence with respect to *k*-point sampling density and kinetic energy cutoff of the plane wave basis for bulk α-Al_2O_3 and fcc Al structures. As a result of these convergence tests, we employed a *k*-point sampling of $3 \times 3 \times 1$ for the hexagonal unit cell of Al_2O_3 and $8 \times 8 \times 8$ for the bulk fcc cell of Al. For both sets of calculations, we used the same kinetic energy cutoff of 338 eV for the planewave basis and 554 eV for the augmentation charge basis needed for our ultrasoft pseudopotentials. We optimized the volume of the primitive crystals by performing a series of single point energy calculations uniformly scaling the lattice vectors within ~5% of the equilibrium value and fitting to the Murnaghan equation of state. The optimum bulk cell lattice vectors (which are within ~1% of experiment [C. Rodriguez, O. Cappannini, E. Peltzer y Blanca, R. Casali, *Phys. Status Solidi B* **1987**, *142*, 353–360; H. d'Amour, D. Schiferl, W. Denner, H. Schulz, W. B. Holzapfel, *J. Appl. Phys.* **1978**, *49*, 4411–4416]) were used in the construction of the cells used in crack simulation, with vacuum added beyond these values in the direction perpendicular to the Al (111) and Al_2O_3 (0001) planes, respectively. Test cases for Al with 6, 9, 12, and 15 atomic layers were performed. For Al_2O_3, test cases of 6, 12, and 18 Al_2O_3 units were also investigated. From these calculations, we determined that nine atomic layers for Al and six Al_2O_3 units (~18 atomic "layers") for Al_2O_3 were sufficient to minimize the interaction of the two surfaces across the periodic slab. In the Al calculations, only three atomic layers on either side of the crack were allowed to relax, that is, the atomic coordinates of the center three layers were kept fixed to their bulk values. Tests have shown that this constraint has little effect on the results.

[14] W. C. Mackrodt, R. J. Davey, S. N. Black, R. Docherty, *J. Cryst. Growth* **1987**, *80*, 441–446.

[15] a) I. Manassidis, A. De Vita, M. J. Gillan, *Surf. Sci. Lett.* **1993**, *285*, L517–L521; b) I. Manassidis, M. J. Gillan, *J. Am. Ceram. Soc.* **1994**, *77*, 335–338.

[16] M. Causà, R. Dovesi, C. Pisani, C. Roetti, *Surf. Sci.* **1989**, *215*, 259–271.

[17] P. W. Tasker in *Advances in Ceramics*, Vol. 10 (Ed.: W. D. Kingery), **1984**, p. 176.

[18] S. Blonski, S. H. Garofalini, *Surf. Sci.* **1993**, *295*, 263–274.

[19] A. M. Rodríguez, G. Bozzolo, G. Ferrante, *Surf. Sci.* **1993**, *289*, 100–126.

[20] J. Schöchlin, K. P. Bohnen, K. M. Ho, *Surf. Sci.* **1995**, *324*, 113–121.

[21] J. R. Smith, G. Bozzolo, A. Banerjea, J. Ferrante, *Phys. Rev. Lett.* **1989**, *63*, 1269–1272.

[22] R. M. Lynden-Bell, *Surf. Sci.* **1991**, *244*, 266–276.

[23] P. A. Taylor, J. S. Nelson, B. W. Dodson, *Phys. Rev. B* **1991**, *44*, 5834 – 5841.
[24] A. Banerjea, B. S. Good, *Int. J. Mod. Phys. B* **1997**, *11*, 315 – 335.
[25] W. Kohn, J. R. Onffroy, *Phys. Rev. B* **1973**, *8*, 2485 – 2495.
[26] J. J. Rehr, W. Kohn, *Phys. Rev. B* **1974**, *10*, 448 – 455.
[27] P. Ordejón, *Comput. Mater. Sci.* **1998**, *12*, 157 – 191.
[28] J. S. Nelson, B. W. Dodson, P. A. Taylor, *Phys. Rev. B* **1992**, *45*, 4439 – 4444.
[29] J. Ferrante, J. R. Smith, *Phys. Rev. B* **1979**, *19*, 3911 – 3920.
[30] S. Ismail-Beigi, T. A. Arias, *Phys. Rev. Lett.* **1999**, *82*, 2127 – 2130.
[31] J. H. Rose, J. R. Smith, J. Ferrante, *Phys. Rev. B* **1983**, *28*, 1835 – 1845.
[32] H. Schlosser, J. Ferrante, J. R. Smith, *Phys. Rev. B* **1991**, *44*, 9696 – 9699.
[33] U. Dürig, O. Züger, L. C. Wang, H. J. Kreuzer, *Europhys. Lett.* **1993**, *23*, 147 – 152.
[34] U. Dürig, *IBM J. Res. Dev.* **1994**, *38*, 347 – 366.
[35] Hypersonic cracks may be an exception: F. F. Abraham, H. Gao, *Phys. Rev. Lett.* **2000**, *84*, 3113 – 3116.

Fractal Growth Patterns in Liquid Crystals**

Ingo Dierking*[a]

KEYWORDS:

crystal growth · fractals · liquid crystals · phase transitions

Fractal geometry is nowadays employed in many branches of science, from physics, chemistry and biology to engineering and geology. It can be used in the description of percolation systems, growth models, material fracture or surfaces and interfaces, to name just a few of its applications. For an introduction on general topics of fractals and disordered systems, see references [1, 2]. In the area of liquid crystal (LC) research, fractal analysis has been employed in the study of the Saffman – Taylor instability in Hele-Shaw cells.[3–6] Patterns formed in viscous fingering were found not to be fractal, while their perimeter was. An estimation of the fractal dimension of a dendritic-type texture of a discotic columnar – hexagonal ordered phase was reported in reference [7]. Other investigations were related to the

[a] *Dr. I. Dierking*[+]
Department of Physics
Chalmers University of Technology
41296 Göteborg (Sweden)

[+] *Present address:*
Institut für Physikalische Chemie
Technische Universität Darmstadt
Petersstrasse 20, 64287 Darmstadt (Germany)
Fax: (+ 49) 6151-16-4924
E-mail: dierking@hrz2.hrz.tu-darmstadt.de

distribution of nuclei[8] and topological defects[9, 10] in nematic LCs and patterns formed at the traveling TGB-SmA* interface.[11] Liquid crystal-related topics having been treated by fractal analysis include burn patterns formed during dielectric breakdown of liquid crystal cells,[12] characterisation of polyimide in Langmuir – Blodgett films for alignment layers[13] and an AFM topology study of SiO substrate layers used for bistable anchoring of nematic LCs.[14]

In this study, the phase-ordering process of the liquid crystalline B2 phase from the isotropic melt is studied with respect to the occurrence and development of fractal growth patterns.

The compound under investigation is a bent-core or so called banana molecule, with the structure given by **1**.
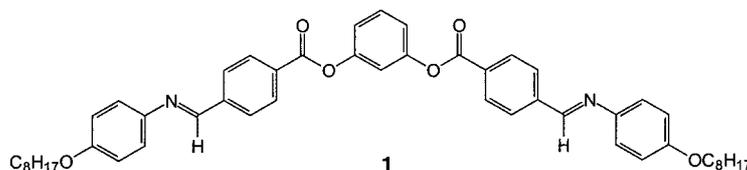
Its phase-transition temperatures, as determined in this study by polarising microscopy on cooling, are Iso. 169.6 B2 150.3 BX 145.5 Cryst. (all temperatures in degrees Celsius). These vary from the originally reported transition temperatures,[15] which is, however, of no relevance to the present investigations. In this study, we are only concerned with the transition from the isotropic phase to the liquid crystalline B2 phase. The transition enthalpy for Iso. →B2 was determined by differential scanning calorimetry to be $\Delta H = 5.7$ kJ mol^{-1}.[15] The B2 phase is a fluid smectic phase of C_{2v} symmetry. It has recently attracted much attention, due to its polar order and antiferroelectric switching behavior, despite the fact that the constituent molecules are achiral.[16] For further details on banana molecules, phase structure and properties, refer to a recent review by Pelzl et al.[17]

The compound does show a rather broad two-phase region on the formation of the liquid crystalline phase of about 3 K, which is quite common for bent-core mesogens. As the sample is not a mixture of different components, this is attributed to impurities contained within the LC. Here, the transition temperature was taken as the one where first germs of the B2 phase were observed within the isotropic melt on very slow cooling.

For the determination of the fractal dimension *D*, several different methods were employed, as listed below.[1, 2, 18]

1) The box-dimension method, where the fractal dimension D_b is given by the exponent in the proportionality in Equation (1), with *N(d)* representing the number of boxes of size *d* occupied by the data set.

$$N(d) \sim \frac{1}{d^{D_b}} \qquad (1)$$

2) The information-dimension method, which defines the fractal dimension D_i from the proportionality in Equation (2).

$$I(d) \sim -D_i \log(d) \qquad (2)$$